J. Anat. (2007) **210**, pp761–766 doi: 10.1111/j.1469-7580.2007.00732.x

METHODS

A model for clubfoot based on micro-CT data

Gunther Windisch,[1] Dietmar Salaberger,[2] Walter Rosmarin,[1] Johann Kastner,[2] Gerhard Ulrich Exner[3], Verena Haldi-Brändle[3] and Friedrich Anderhuber[1]

[1]*Institute of Anatomy Graz, Medical University Graz, Austria*
[2]*Upper Austria University of Applied Science, Wels Campus, Austria*
[3]*Department of Orthopaedics,Universitätsklinik Balgrist, Zurich, Switzerland*

Abstract

The pathological anatomy of idiopathic clubfoot has been investigated for more than 180 years using anatomy, computed tomography (CT), histology and microscopy. Seven idiopathic clubfeet and two normal feet of aborted fetuses were dissected in the present study, with special emphasis on the shape of the cartilage and bones. A three-dimensional (3D) micro-CT system, which generates a series of X-ray attenuation measurements, was used to produce computed reconstructed 3D data sets of each of the separated bones. Based on the micro-CT data scans a high-definition 3D colour printing system was used to make a four times enlarged clubfoot model, precisely presenting all the bony malformations. This model reflects the complexity of the anatomy of this disease and is designed to be used in the workshops of orthopaedic surgeons and physiotherapists, for training in new surgical and manipulation techniques.

Key words 3D printer; clubfoot; micro-CT; model.

Introduction

Idiopathic clubfoot is a variable three-dimensional (3D) deformity of a complex system of bones, joints, and their adjacent ligamentous and muscular stabilization systems. It occurs in approximately one in every 1000 births (Fig. 1).

The pathological anatomy and the structural changes of the bones were first described more than 180 years ago, and many theories have been proposed to explain the aetiology and pathogenesis. Scarpa (1818) suggested the osseous deformities of the talus as the primary cause, and this was confirmed by Irani & Sherman (1963). Böhm (1929) believed that clubfoot results from an arrest of development at the clubfoot embryonal stage that usually does not exist in normal embryos. A regional growth disturbance was postulated by Dietz et al. (1983), who studied the posterior tibial tendon sheath in clubfeet and normal feet. Shortening of the muscles of the leg and muscular fibrosis have been frequently reported (Schlicht, 1963). Fritsch & Eggers (1999) showed that, in clubfoot calcaneus, the precise sequence of calcaneal ossification is disturbed, and that the first perichondral ossification centre is not situated laterally but inferiorly or medially. In two studies the authors presumed that the disturbance of ossification of the calcaneus is the primary fault because of its periosteal ossification is noted before that of the talus (Windisch et al. 2007a,b).

These different views have engendered many discussions which further emphasize the existing differences of operative treatments. What is not in doubt is that the functional anatomy is a prerequisite to achieving an aligned and supple foot with a good prognostic value, regardless of different orthopaedic treatment techniques.

The aim of our study was to increase our understanding of the 3D complexity of the idiopathic clubfoot by the use of a clubfoot model. The 3D data sets presented were scanned using an industrial 3D micro-computed tomography (micro-CT) system. The main advantages

Correspondence
Gunther Windisch, MD, Institute of Anatomy, Medical University Graz, Austria, Harrachgasse 21, 8010 Graz, Austria, Europe.
T: 0043 316380 7582; F: 0043 316380 69 7582;
E: gunther.windisch@meduni-graz.at

Accepted for publication *9 March 2007*

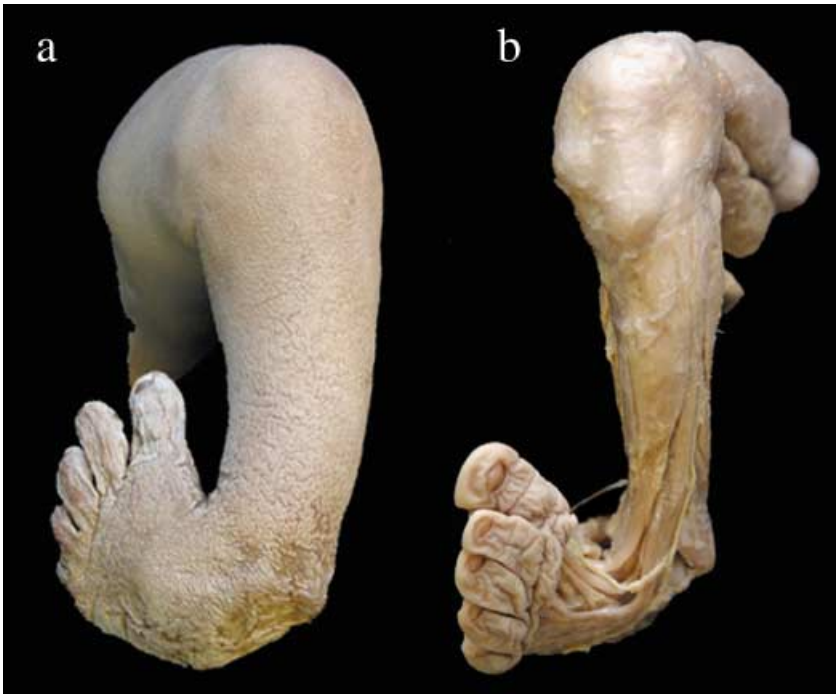

Fig. 1 Clubfoot grade IV before (a) and after dissection (b). Anterior view of a grade IV clubfoot according to the Diméglio/Bensahel score showing the malformation of the foot. All specimens were dissected layer by layer to examine all changes in muscles, tendons and joints (b).

of the system were the high scanning speed and the high resolution, enabling us to locate and measure volumetric details in three dimensions.

Based on these data, surface models were generated. A clubfoot model and a model of a normal foot were created based on a high-performance composite on a 3D printer.

Dissected idiopathic clubfoot specimens had not previously been available for micro-CT scan. The model was magnified four times to get the best impression of the complex pathoanatomy, and we believe that the model will be used in orthopaedic surgery and physiotherapy workshops, for training in new surgical and manipulation techniques.

Methods

Anatomy

Surgical exposure on seven idiopathic clubfeet of fetuses aborted between the 25th and 37th week of gestation was made by the use of magnifying loupes and compared with two normal feet (27th and 36th week of gestation). These clubfeet were embalmed according to Thiel's method, which preserves the natural character of the tissues and allows joint motion (Thiel, 1992). For classification we used the Diméglio/Bensahel score, which considers four essential multiple parameters (Diméglio et al. 1995): (1) equinus deviation in the sagittal plane, (2) varus deviation in the frontal plane, (3) inversion/eversion in the subtalar and talocalcaneonavicular joint, and (4) adduction of the forefoot relative to the hind foot in the horizontal plane.

According to these parameters, four categories of clubfoot can be identified in increasing order of severity: (a) benign (grade I), (b) moderate (grade II), (c) severe (grade III) and (d) very severe (grade IV).

We dissected three feet with grade IV clubfoot, two with grade III, one with grade II and one with grade I. The joints were disarticulated to determine the articular surfaces and the shape of the bones and cartilage. The clubfoot model was made of the dissected grade IV specimen to show the 3D complexity of this disease. We used a very severe clubfoot (grade IV) and a normal foot, and each of the following bones were scanned and printed separately: tibia and fibula, talus, calcaneus, cuboid, navicular, the three cuneiforms and the five metatarsals.

Computed tomography scans

Over the past few years X-ray CT has been applied in industrial situations. In the automobile and aeronautic industries, equipment is tested non-destructively during development to improve the manufacturing process (Simon & Sauerwein, 2000).

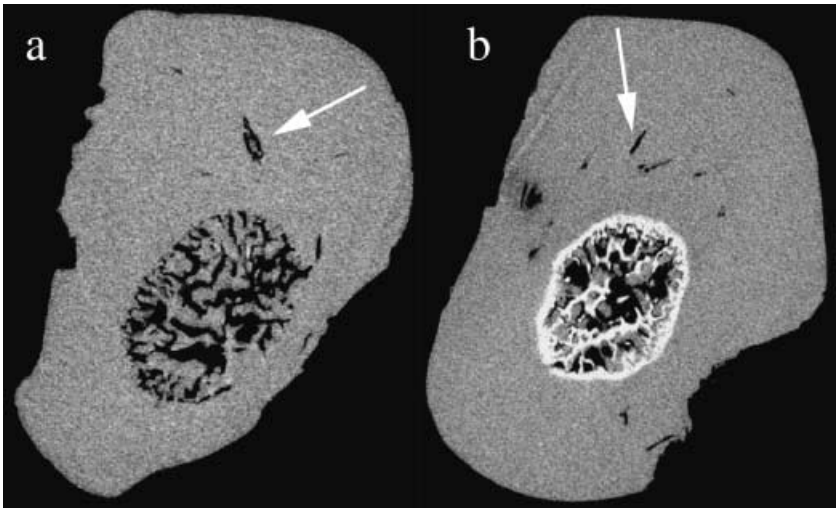

Fig. 2 Slice image through the 3D data set of the tali. The cartilage canals (arrows), which are involved in nutrition, chondrogenesis and osteogenesis, are presented. They enter the cartilage from the perichondrium and join the ossification centre. After the scanning process all inner structures had to be removed before the surface extraction was performed.

Due to various differences in equipment and scanning procedures, industrial computed tomographs have two main advantages over medical ones. One advantage is the high isotropic spatial resolution (down to 5 μm). The other is the fact that even high-density materials like aluminium or steel can be irradiated (Kastner et al. 2005).

Since X-ray CT was originally a medical diagnostic imaging method it is well suited to investigating bone specimens.

The scans were made at the Upper Austria University of applied science in Wels, where an industrial 3D computed tomography device, Ray Scan 250 E (Hans Wälischmiller GmbH, Meersburg, Germany), has been available since November 2004 (Kastner et al. 2006).

The spatial resolution is determined by the size of each volumetric pixel (voxel) of the data set. For each bone the optimal voxel size was set, given that the specimen dimension determines the voxel size. The calf of the leg was scanned at 47.2 μm, the metatarsals at 27.2 μm, the calcaneus at 24 μm, the talus at 20 μm, the navicular and cuboid at 20.7 μm, and the cuneiforms at 17 μm voxel size (Fig. 2).

Surface extraction

In order to extract a valuable surface model of the grey value data set, common surface creation algorithms are used. Usually a single isovalue is specified to distinguish between the material and air. For example, the matching cubes algorithm creates triangle models of constant density surfaces from 3D volume data (Lorensen & Cline, 1997). The isovalue can be generated automatically by Otsu's global thresholding method, or manually by trial and error (Otsu, 1979). The result of this process is a surface representation of the specimen, with stereo lithography file format (STL) data sets. To preserve the fine detail, the resulting polygonal mesh consists of up to 1.5 million triangles for a single bone (Fig. 3).

For each CT measurement, a suitable threshold was determined by choosing half the grey value between the air and the bone. Surface extraction was performed with the 3D data evaluation software VG Studio Max 1.2 (Volume Graphics, Heidelberg, Germany).

3D printing

Rapid prototyping tools may be used to construct physical models or prototypes very rapidly, directly from virtual data sets such as computer-aided design (CAD), magnetic resonance tomography (MRT) or CT data sets. These technologies are employed as a way of reducing time to market in manufacturing, to allow better understanding and communicating of product designs, and for faster tooling during the manufacturing process.

For the 3D printing of our clubfoot and normal foot, we used a special application called the Spectrum Z 510 3D printer (Z Corporation, Burlington, MA, USA). This 3D printer creates physical models from CAD data by using an inkjet print head to deposit a liquid binder that solidifies the layers of powder.

To get a solid model with a smooth surface, the extracted STL data sets need further treatment. Automatic

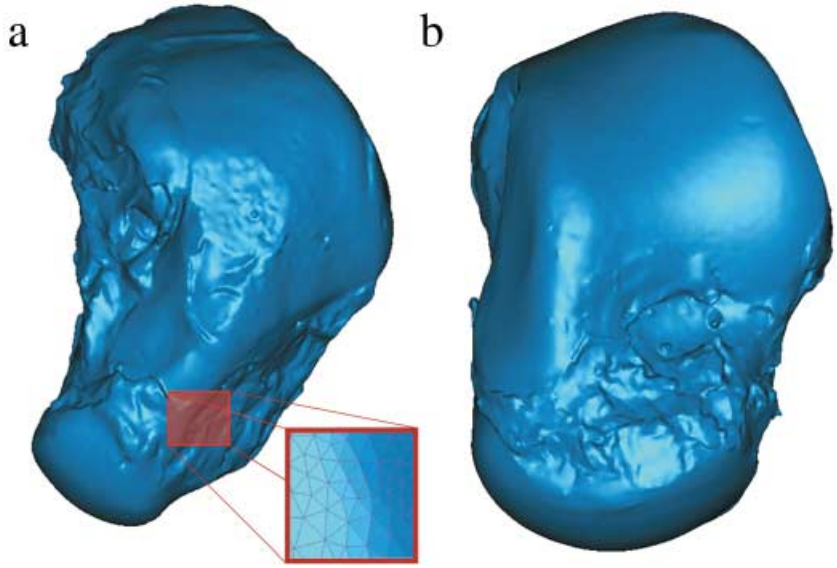

Fig. 3 STL data sets of clubfoot talus (a) and normal talus (b). After surface extraction the surface represents a polygonal mesh consisting of up to 1.5 million triangles.

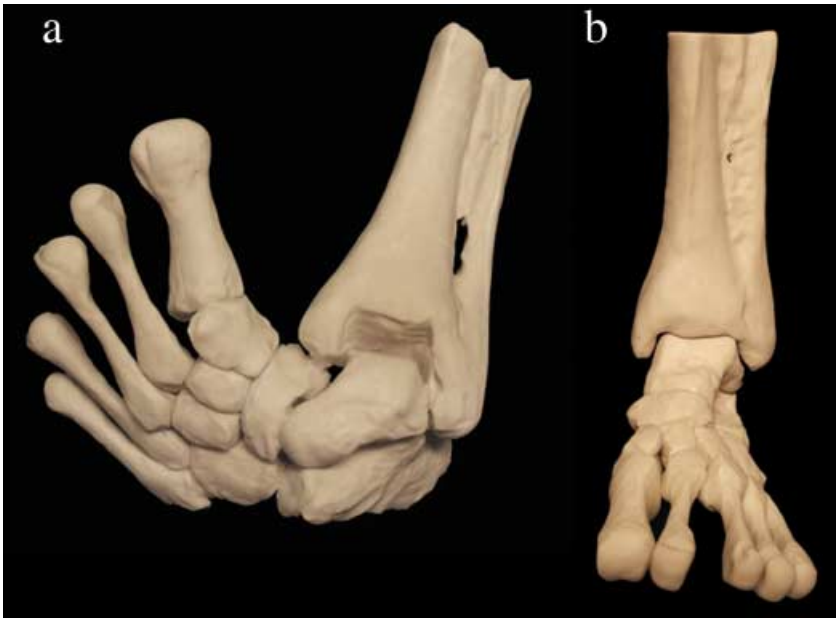

Fig. 4 Constructed models of (a) clubfoot and (b) normal foot. After the 3D printing of each bone the models were stuck together with glue. The different shape of the malformed bones as well as the position of the bones in all joints is clearly demonstrated. The enlargement of the models makes it easier to understand the complexity of this disease.

procedures such as smoothing, noise reduction and closing holes were applied. In regions of joint surfaces these procedures will not change the geometry of the surface more than a few micrometres.

As the geometrical structures are represented virtually in software data sets, the printed models can be scaled up or down. To gain a better impression of the differences in geometry of joint surfaces and bone configuration between the normal and pathological foot, a scale of 4 : 1 was used. The printed models thus generated represent a size similar to an adult foot (Fig. 4).

Results

With the 3D printer, we enlarged four-fold the images of the calf of the leg, talus, calcaneus, navicular, cuboid, three cuneiforms and five metatarsal bones in the normal foot as well as the clubfoot. With these bones a model of a clubfoot and a model of a normal foot were made. The magnified clubfoot model precisely demonstrated the malformation of each bone and the 3D complexity associated with this disease (Fig. 4).

Discussion

Increasingly, skeletal models of the human body are being used as powerful tools for studying biological structures; however, they frequently lack the geometric detail necessary to provide meaningful insights into biomechanical behaviour. Several models of the human foot have been developed in an attempt to clarify our understanding of biomechanics. A knowledge of bone motion and functional anatomy are necessary for understanding gait as well as foot pathologies such as clubfoot. In previous studies some bones of the clubfoot were studied to evaluate the morphological deformity by use of magnetic resonance. Based on the resulting magnetic resonance imaging volume data, 3D surface models were reconstructed (Kamegaya et al. 2001; Cahuzac et al. 2002; Saito et al. 2004; Itohara et al. 2005a,b). 3D motion of the entire hind foot was evaluated by Roche et al. (2005) and Mattingly et al. (2006) using virtual 3D models to establish a new and quantitative objective.

Camacho et al. (2002) generated a 3D reconstruction of a human foot from CT images. A 3D surface model was made, and a detailed 3D mesh for each bone was created. The model was used to quantify foot shape using the relationship between the principal axes of the bones.

This was the first study in which micro-CT was used for clubfoot specimens. It was also the first time that clubfoot bones had been scanned and printed separately, in order to exclude any lack of details concerning the joint surface; in fact this is the most important part in the understanding and treatment of this disease.

Images of all bones were enlarged four times and printed to get all necessary details required to study individual movements of the bones in clubfeet. These data show how complex this disease is anatomically. In addition, the enlarged model will be of great use for orthopaedic surgeons and physiotherapists, in enabling them to get the best impression of the malformed bones and to develop and practise new surgical and manipulation techniques.

References

Böhm M (1929) The embryologic origin of club-foot. *J Bone Joint Surg* **11**, 229–259.

Cahuzac JP, Navascues J, Baunin C, et al. (2002) Assessment of the position of the navicular by three-dimensional magnetic resonance imaging in infant foot deformities. *J Pediatr Orthop* **11**, 134–138.

Camacho DL, Ledoux WR, Rohr ES, Sangeorzan BJ, Ching RP (2002) A three-dimensional, anatomically detailed foot model: a foundation for a finite element simulation and means of quantifying foot-bone position. *J Rehabil Res Dev* **39**, 401–410.

Dietz FR, Ponseti IV, Buckwalter JA (1983) Morphometric study of clubfoot tendon sheaths. *J Pediatr Orthop* **3**, 311–318.

Diméglio A, Bensahel H, Souchet PH, Mazeau PH, Bonnet F (1995) Classification of clubfoot. *J Pediatr Orthop* **4**, 129–136.

Fritsch H, Eggers R (1999) Ossification of the calcaneus in the normal fetal foot and in clubfoot. *J Pediatr Orthop* **19**, 22–26.

Irani RN, Sherman MS (1963) The pathological anatomy of clubfoot. *J Bone Joint Surg Am* **45**, 45–52.

Itohara T, Sugamoto K, Shimizu N, et al. (2005a) Assessment of talus deformity by three-dimensional MRI in congential clubfoot. *Eur J Radiol* **53**, 78–83.

Itohara T, Sugamoto K, Shimizu N, et al. (2005b) Assessment of the three-dimensional relationship of the ossific nuclei and cartilaginous anlagen in congenital clubfoot by 3D MRI. *J Orthop Res* **23**, 1160–1164.

Kamegaya M, Shinohara Y, Kuniyoshi K, Moriya H (2001) MRI study of talonavicular alignment in club foot. *J Bone Joint Surg Br* **83**, 726–730.

Kastner J, Schlotthauer E, Salaberger D, Simon M, Sauerwein C (2005) *Mikro-Computertomographie für die Charakterisierung und Vermessung von Mikrobauteilen*. Rostock, Germany: Jahrestagung der DGZfP.

Kastner J, Heim D, Salaberger D, Sauerwein C, Simon M (2006) Advanced applications of computed tomography by combination of different methods. In *9th European Conference on Non-Destructive Testing, Proceedings CD, Berlin, Germany*.

Lorensen W, Cline H (1997) Marching cubes: a high resolution 3D surface construction algorithm. *ACM SIGGRAPH Computer Graphics* **21**, 163–166.

Mattingly B, Talwalkar V, Tylkowski C, Stevens DB, Hardy PA, Pienkowski D (2006) Three-dimensional in vivo motion of adult hind foot bones. *J Biomech* **39**, 726–733.

Otsu N (1979) A threshold selection method from grey level histograms. *IEEE Trans Systems Man and Cybernetics*, **9**.

Roche C, Mattingly B, Md VT, et al. (2005) Three-dimensional hindfoot motion in adolescents with surgically treated unilateral clubfoot. *J Pediatr Orthop* **25**, 630–634.

Saito S, Hatori M, Kokubun S, Abe Y, Kita A (2004) Evaluation of calcaneal malposition by magnetic resonance imaging in the infantile clubfoot. *J Pediatr Orthop B* **13**, 99–102.

Scarpa A (1818) *A Memoir on the Congenital Club Feet of Children, and on the Mode of Correcting that Deformity*. Translated from Italian by J. H. Wishart. Edinburgh: Constable.

Schlicht D (1963) The pathological anatomy of talipes equinovarus. *Aust NZ J Surg* **33**, 1–11.

Simon M, Sauerwein C (2000) Cone beam tomography for quality control and rapid product development. *Insight* **42**, 651–654.

Thiel W (1992) Die Konservierung ganzer Leichen in natürlichen Farben [the Preservation Whole Corps with Natural Color]. *Ann Anat* **174**, 185–195.

Windisch G, Anderhuber F, Haldi-Brändle V, Exner GU (2007a) Anatomical study for an update comprehension of clubfoot. Part I: bones and joints. *J Child Orthop* online version: http://www.springerlink.com/content/1863-2548. doi 10.1007/s11832-006-0003-3

Windisch G, Anderhuber F, Haldi-Brändle V, Exner GU (2007b) Anatomical study for an update comprehension of clubfoot. Part II: ligaments, tendons and muscles. *J Child Orthop* online version: http://www.springerlink.com/content/1863-2548. doi 10.1007/s11832-006-0004-2